Journal of

Materials Chemistry C

RSCPublishing

ARTICLE

Synthesis and magnetic properties of Ni-$BaTiO_3$ nanocable arrays within ordered anodic alumina templates

Cite this: DOI: 10.1039/x0xx00000x

D.Sallagoity [ab], C. Elissalde [a], J. Majimel [a], R. Berthelot [c], U. Chan Chung [a], N. Penin [a], M. Maglione [a], Vlad. A. Antohe [b], G. Hamoir [b], F. Abreu Araujo [b], and L. Piraux [b]

Received ooth January 2012,
Accepted 00th January 2012

DOI: 10.1039/x0xx00000x

www.rsc.org/

A reliable and flexible synthesis route was used for processing high density Ni-$BaTiO_3$ nanocables array based on wet chemical impregnation and subsequent electrodeposition within a highly ordered unidirectional porous alumina membrane. The core-shell structure was carefully investigated by Bright field Scanning Transmission Electronic Microscopy coupled with Energy Dispersive X-Ray Spectroscopy. The strength of the dipolar interaction arising from the packing density of the magnetic nanowires was correlated to the $BaTiO_3$ wall thickness through magnetometry and ferromagnetic resonance measurements. Our approach opens a pathway to perform optimized nanostructured multiferroic composites exhibiting tunable magnetic properties.

Introduction

One-dimensional magnetic nanostructures have been paid great attention in different research fields due to their unique properties and their possible exploitations in relevant applications, such as patterned media for magnetic storage[1,2], non-reciprocal microwave devices[3-5], spintronics devices[6-9] and biomedecine[10,11]. To tailor the physical properties of 1D nanostructures to a more diverse range, heterostructures that combine two or more materials with different magnetic and electric properties in a radial structure opens new perspectives towards the elaboration of multiferroic composite materials. In this regard, the coexistence and coupling between the ferromagnetic and ferroelectric properties may lead to the attractive electric control of the magnetic properties. Tuning the properties of such ferromagnetic core nanowires (NWs) through their interactions with the ferroelectric shell is of interest for developing microwave devices and metamaterial structures with enhanced electrical tunability of their operating frequency[12,13].

Multiferroic composites consisting of arrays of magnetic nanowires surrounded by a ferroelectric material have been synthesized using various methods, such as sputtering[12], electrospinning[14,15] and template assisted growth techniques[16-20]. There is a growing interest in the use of template synthesis due to its flexibility and reliability performances. Only few works along this line involved a combination of wet impregnation and electrodeposition to elaborate core-shell nanocables comprising a ferromagnetic metal[20] or oxide[18] core surrounded by a dielectric oxide shell in anodic aluminium oxide (AAO) nanoporous membranes. The versatility of this approach lies in the tunability of the nanocable length, the core diameter, the ferroelectric tube wall thickness, and consequently the packing density of the magnetic nanowires. However a detailed structural and morphological study was not yet reported. Well-designed coaxial heterostructures are required to achieve, desired properties and functionalities.

In this work, we used the combination of wet chemical oxide impregnation and subsequent metal electrodeposition process into AAO to elaborate high density array of coaxial nanocables, made of Ni ferromagnetic nanowires surrounded by $BaTiO_3$ (BTO) dielectric nanotubes (NTs). We propose a complete description of our Ni-BTO nanocomposites using electron microscopy and magnetic characterization using Superconducting Quantum Interference Device (SQUID) and Ferromagnetic Resonance (FMR) measurements. We investigate the influence of the wall thickness of the BTO NTs on the magnetic properties of the coaxial nanocable arrays.

Experimental section

Commercial AAO templates (Synkera Technology Inc., Longmont, CO, USA) were used as the host membrane. These membranes have narrow pore distribution and excellent thermal and chemical stability. Arrays of pure Ni NWs have been fabricated by direct electrodeposition in AAO membranes having a thickness of 50 µm with pore diameter of 150 nm, inter-pore distance (the center to center distance between pores) of 210-220 nm and porosity

(P) of 30%. The system used is a three-electrode system with Pt foil as anode electrode and an Ag/AgCl electrode as reference electrode. A Cu layer was evaporated on one side of the membrane in order to cover the pores and use it as a cathode. Ni NWs were grown at a constant potential of −1.1 V *vs.* Ag/AgCl from a 1M $NiSO_4 \cdot 6H_2O$ + 0.5M H_3BO_3 electrolyte at ambient temperature. The plating current is recorded as a function of time and the electrodeposition process is stopped before the wires emerge from the surface, as evidenced by a sudden increase of the plating current.

Arrays of Ni-BTO nanocables were elaborated using a multi-step process consisting of sol-gel impregnation, thermal annealing and crystallisation of BTO NTs followed by Ni electrodeposition within the pore walls of the AAO templates coated with BTO (see Scheme 1).

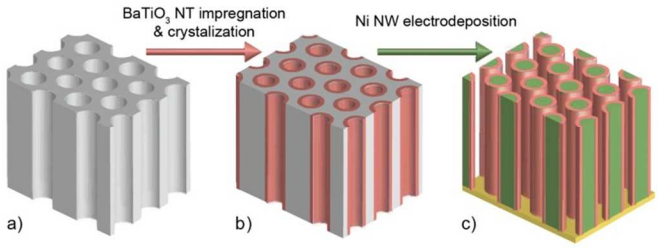

Scheme 1. (Color online) Ni-$BaTiO_3$ nanocable multistep synthesis.

The BT sol was synthesized using barium acetate $Ba(CH_3CO_2)_2$ and titanium (IV) isopropoxide $Ti(OCH(CH_3)_2)_4$ from Sigma Aldrich as precursors[21]. Subsequently, $Ba(OAc)_2$ was dissolved in glacial acid acetic at 80°C under magnetic stirring. Titanium was dissolved in a second vessel containing isopropanol at room temperature under stirring. Then the two solutions were mixed under stirring at room temperature to form an homogeneous 0.4M stoichiometric BT sol. AAO templates were immersed into the BT sol during one minute. Wet faces were carefully dried with absorbant paper to remove the BT film formed on the top, before the crystallization annealing. The calcination temperature was also strictly limited to 700°C in order to avoid membrane film curvature and the phase transformation of amorphous alumina into α-Al_2O_3 (onset at 860°C as shown by thermal analysis). These points are crucial but rarely underlined in the literature : such an alumina crystallization have detrimental effects for several reasons: i) it can affect BTO microstructure through surface rearrangement and interdiffusion across interfaces, ii) only amorphous alumina can be completely removed in NaOH to allow an unambiguous characterization of the BTO nanotubes[22], and the membrane film curvature prevents the subsequent Ni electrodeposition into the AAO templates coated with BTO from occuring. The uniform growth of the Ni nanowires was stopped before the nanowires reach the surface of the AAO template to preserve the one-dimensional core-shell shape. Ferromagnetic resonance (FMR) measurements at room temperature have been done in the field swept mode using a microstrip transmission line with an external magnetic field applied parallel to the revolution axis, as reported previously for NWs within porous templates[23]. Room temperature magnetometry measurements were performed using a Quantum Design SQUID Magnetometer.

Results and discussion

SEM investigations (10kV) were first carried out to check the BTO NTs structure after the removal of alumina template with 1M NaOH(aq) solution (see Fig. 1(a)). Bundle of thin NTs with a high aspect ratio are formed driven by strong interactions between the hydrophilic surfaces of adjacent BTO NTs. Holes and asperities are identified on the surface of the NTs.

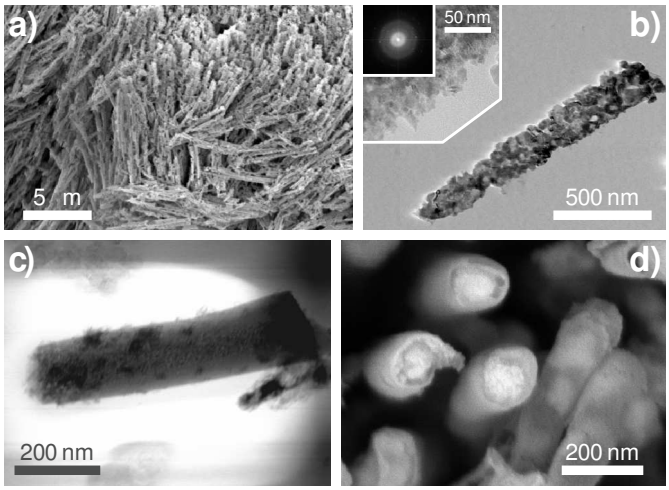

Figure 1. (a) SEM picture of $BaTiO_3$ nanotube bundle after the removal of the alumina template. (b) HRTEM micrograph of a fractured nanotube (zoom on individual crystallites with digital diffractogram illustrating the polycrystalline organization in inset). (c) HRTEM micrograph of a single Ni nanowire. (d) SEM image of Ni-$BaTiO_3$ core-shell nanocables.

It can be explained by the partial dissolution of barium species during the etching process (Ba-rich well defined micrometric hexagonal objects can appear when NaOH concentration is higher than 1M). TEM measurements (200 kV) were performed after the template removal and ultrasonic dispersion in ethanol (see Fig. 1(b)). The BTO NTs collected are usually broken in several segments with lengths of a few micrometers. They consist of fine-grained polycrystalline materials with a compact texture as confirmed by the diffraction pattern exhibiting a series of concentric rings (see inset in Fig. 1(b)). The BTO NTs have grain sizes in the range 20-30 nm and grains have no preferential orientation with respect to the tube axis. Ni NWs with a few micrometers in length were also observed by HRTEM (see Fig. 1(c)). The electrodeposited Ni NWs appear nanometer-sized (5-10nm) polycrystalline materials with no preferential orientation along the wire axis. This is confirmed by XRD measurements (not shown) in agreement with a previous study on electrodeposited Ni NWs [24]. The polycrystalline nature of the Ni NWs with small grains is also evidenced by the high resolution SEM image of core-shell NWs shown in Fig. 1(d). The diameter of the metallic core is about 90-100 nm, while the thickness of the shell is 20-30 nm.

Bright field scanning transmission electron microscopy (STEM) experiments coupled with Energy Dispersive X-ray Spectroscopy (EDX) analyses were performed on Ni-BTO core-shell nanowires after grinding and dispersion in ethanol (Fig. 2(a, b)). EDX profiles across Ba, Ti and Ni rich areas (Fig. 2(c)) can be compared with the total projected thickness of a nanotube along the direction of the electron beam (t) described by the following Eqs :

$$t = \sqrt{r_0^2 - r^2} - \sqrt{r_i^2 - r^2} \; ; r < r_i \quad (1)$$

$$t = \sqrt{r_0^2 - r^2} \; ; r < r_i \quad (2)$$

where r_o and r_i represent the outer and the inner radii of the BTO tubes respectively. The experimental data are found to be in good agreement with the calculated profile that confirms the nanotube shape for BTO. On the contrary, Ni chemical profile exhibits a single maximum in the core region of the BTO tube which reveals clearly the core-shell structure. The mean tube wall thickness is about 30 nm in agreement with the crystallite size estimated in Fig. 1(b), and the core diameter is close to 90 nm. The core-shell morphology is also confirmed from the EDS mapping performed on isolated Ni-$BaTiO_3$ NWs, as shown in Fig. 2(d).

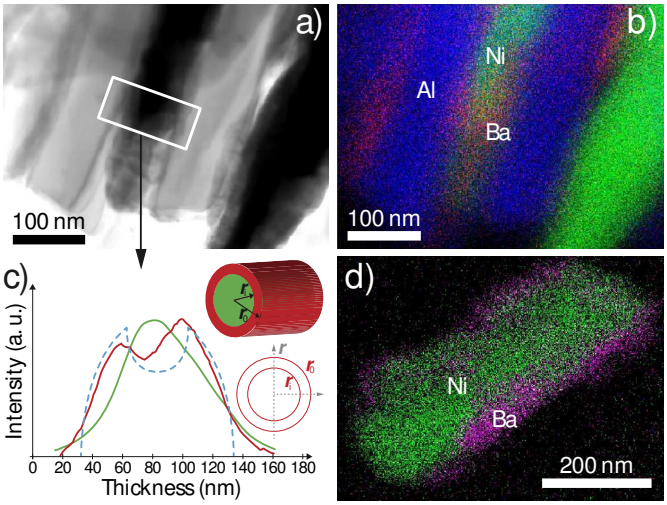

Figure 2. (Color online) (a) Bright field STEM micrograph of Ni-$BaTiO_3$ core-shell architecture within the template after grinding and dispersion in EtOH. (b) Chemical mapping of the area in (a), with Ba, Ni and Al in red, green, blue respectively. (c) EDX profiles integrated along the marked area in (a), with (Ba, Ti) and Ni in red, green respectively; blue refers to the simulation of total BTO tube projected along the electron beam direction for a 30nm wall thickness tube into a 150 nm diameter pore. (d) BF-STEM micrograph of an isolated Ni-$BaTiO_3$ core-shell after template removal.

For Ni NWs and Ni-BTO nanocables ordered arrays within AAO, magnetocrystalline anisotropy (MCA) contributions can be neglected so the effective field H_{eff} in the saturated state contains only the shape anisotropy and the dipolar interaction field. Moreover since both nanowire systems have the same symmetry and for the samples considered here their aspect ratio is large, the same mean field model used for NWs can also be used for core-shell NWs. Therefore, the effective field can be expressed as [25]

$$H_{eff} = 2\pi M_s - 6\pi M_s P \quad (3)$$

where $2\pi M_s$ is the shape anisotropy, $6\pi M_s P$ is the dipolar interaction field in the saturated state and M_s=485 emu.cm^{-3} is the saturation magnetization density for Ni. Due to their different volume, the packing fractions for core-shell system ($P_{Ni\text{-}BTO}$) and nanowires (P_{Ni}) are different and when grown in the same template $P_{Ni\text{-}BTO} < P_{Ni}$. Fig. 3 compares the normalized hysteresis loops measured at room temperature with the field applied along the revolution axis of the NWs. A clear difference is observed between the two samples, in particular Ni-BTO core-shell NWs are more easily magnetized than their Ni NWs counterpart. The main differences observed in their hysteresis loops arise from their respective effective fields and in particular from the dipolar interaction field. Indeed, as mentioned above $P_{Ni\text{-}BTO} < P_{Ni}$, which as seen from the second term in Eq. (3) results in a smaller interaction field and thus a higher effective field and a stronger uniaxial anisotropy in core-shell NWs. Moreover, the high packing values of the templates results in a strong dipolar interaction which is responsible for the shearing of the hysteresis loops and their reduced squareness. This shearing depends on the value of the dipolar interaction field so the hysteresis loops of NWs are more sheared than those measured in core-shell NWs[26]. It is also noted that nanowires and nanocables systems exhibit similar coercive fields (around 250 Oe).

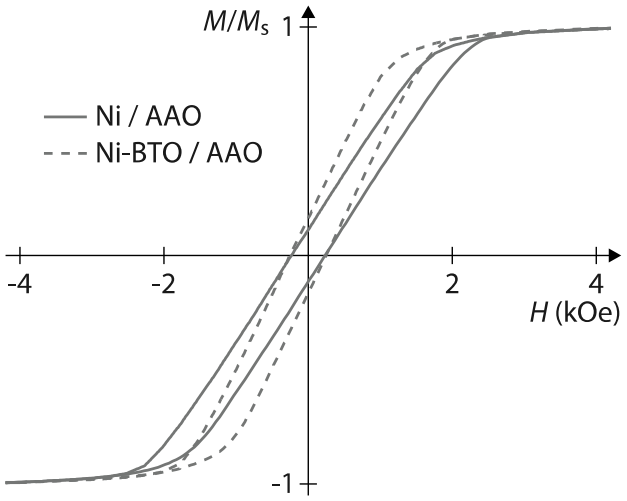

Figure 3. (Color online) Room temperature hysteresis loops measured along the revolution axis in arrays of Ni nanowires (dashed line) and of Ni-BTO nanocables (solid line) embedded in AAO templates.

In order to have an accurate determination of the effective field H_{eff}, the FMR properties of these core-shell nanowires have been measured. These magnetically-filled porous membranes are particularly well adapted for a simple fabrication of the micro-strip transmission line and the investigation of the ferromagnetic resonance properties at GHz frequencies[25,27]. The microwave signal propagating along the microstrip transmission line deposited on the free surface of the membrane (Fig. 4(a)) produces a microwave pumping field which is perpendicular to the nanowires and induces a precession of the magnetization around the static equilibrium position.
At ferromagnetic resonance, power is absorbed from the incident microwave signal and the corresponding minimum in the transmitted power is recorded by a network analyzer. The analysis of the FMR results is made in the saturation state where the magnetization inside the wires can be considered as single domain. At a given constant frequency f, the ferromagnetic resonance condition when the magnetic field is applied parallel to the wires is [25] :

$$H_r = \frac{f}{\gamma} - H_{eff} \quad (4)$$

where H_r is the resonance field and γ the gyromagnetic ratio (γ ~ 3.09 GHz/kOe for Ni). Figure 4(b) presents a set of transmission spectra obtained at room temperature and recorded at 15 GHz and 25 GHz for both Ni nanowires and Ni-BTO nanocables. From the spectra shown in Fig. 4(b), it can be observed that at the same frequency, the core-shell NWs sample presents lower resonance fields than the reference Ni NWs sample. The shift of the resonance field is about 1.5 kOe and a clear upward displacement of the dispersion relation of the core-shell NWs sample with respect to those of the corresponding Ni NWs is observed. From Eq. (4), it can be seen that at a given frequency, a decrease of the H_r resonance field corresponds to an increase of the effective field in Ni-BTO NWs that result from their lower packing fraction. Figure 4(c) shows their corresponding dispersion relations, where the straight lines correspond to the fit of the experimental data to Eq. (4). Fitting of the experimental data yields the effective field, H_{eff}, and the packing fractions for NWs and NTs in each template. For Ni NWs, we get H_{eff} ~ 0 kOe and P_{Ni} ~ 30% while for Ni-BTO core-shell NWs, we get H_{eff} ~ 1.4 kOe and $P_{Ni\text{-}BTO}$ ~ 16%. Assuming that BTO nanotubes cover homogeneously the wall of the pores, we estimate the wall thickness around 35nm, in agreement with previous electronic microscopy observations.

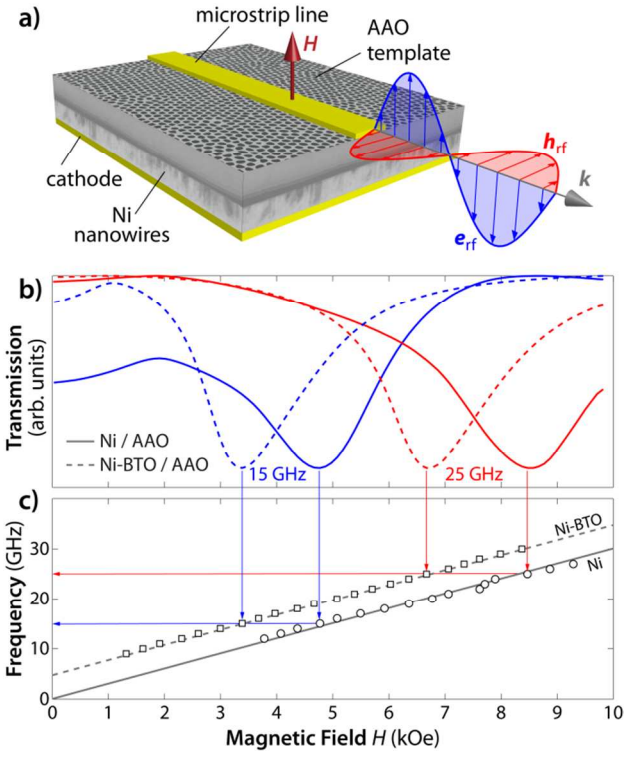

Figure 4. (Color online) a) Schematics of the microstrip transmission line, in which the cathode, or ground plane, is separated from the 150µm-wide microstrip line by a dielectric which corresponds to the AAO membrane containing the nanocables. b) Field sweep microwave absorption spectra obtained at 300K and recorded at 15GHz and 25 GHz with the field applied parallel to the wire axis for arrays of Ni-BTO NWs and Ni NWs grown in AAO. c) The corresponding measured dispersion relations.

Conclusions

In conclusion, we report on a reliable and controllable synthesis method of high-density arrays of coaxial Ni-$BaTiO_3$ nanocables within anodic aluminium oxide membranes. This synthesis approach based on a combination of electrochemical and a sol-gel process allows for modulation of the magnetic properties of core/shell nanowires by an appropriate choice of membrane material, packing fraction, geometric parameters (*i.e.*, core radius and shell thickness) and composition. The detailed investigation of the structural and morphological features of these metal/oxide nanocables is an important step towards the elaboration of one-dimensional multiferroic nanostructures with rigorously tailored architectures. Distorted magnetic hysteresis loops and shifted ferromagnetic resonances are in agreement with the decreased packing of Ni wires in the core-shell nanocables as compared to the nanowires. Further work is under progress to achieve enhanced magnetic/electrical tunability of their properties which is of considerable importance for developing tunable microwave devices and new metamaterial structures.

Acknowledgements

F.A.A. acknowledges the Research Science Foundation of Belgium (FRS-FNRS) for financial support (FRIA grant). The IDS FunMat European doctoral school is acknowledged for financial support.

Notes and references

[a] CNRS, Univ. Bordeaux, ICMCB, UPR 9048, 87 Avenue du Docteur Schweitzer, 33600 Pessac, France.

[b] Institute of Condensed Matter and Nanosciences, Université catholique de Louvain, Place Croix du Sud, B-1348, Louvain-la-Neuve, Belgium.

[c] ICGM-UMR5253, Université Montpellier II, 2 Place Eugène Bataillon, CC 1502, 34095 Montpellier CEDEX 5, France.

1 C. A. Ross, Patterned magnetic recording media, *Annu. Rev. Mater. Res.* 2001, **31**, 203-235.

2 D. Sellmyer, Y. Xu, M. Yan, Y. Sui, J. Zhou and R. Skomski, Assembly of High-anisotropy $L1_0$ FePt Nanocomposite Films, *J. Magn. Magn. Mater.* 2006, **303**, 302-308.

3 J. F.Allaeys, B. Marcilhac, and J. C. Mage, Influence of track-etching on polycarbonate membrane permittivity, *J. Phys. D: Appl. Phys.* 2007, **40**, 3714.

4 M. Darques, J. De La Torre Medina, L. Piraux, L. Cagnon and I. Huynen, Microwave Circulator Based on Ferromagnetic Nanowire in an Alumina Template, *Nanotechnology,* 2010, **21**, 145208.

5 C. E. Carreon-Gonzalez, J. De La Torre Medina, L. Piraux and A. Encinas, Electrodeposition Growth of Nanowire Arrays with Height Gradient Profiles for Microwave Device Applications, *Nano Lett.* 2011, **11**, 2023-2027.

6 L. Piraux, K. Renard, R. Guillemet, S. Matefi-Tempfli, M. Matefi-Tempfli, V. A. Antohe, S. Fusil, K. Bouzehouane and V. Cros, Template-

Grown NiFe/Cu/NiFe Nanowires for Spin Transfer Devices, *Nano Lett.* 2007, **7**, 2563-2567.

7 N. Biziere, E. Mure and J. P. Ansermet, Microwave Spin-torque Excitation in a Template-synthesized Nanomagnet, *Phys. Rev. B,* 2009, ***79*,** 012404.

8 D. Pullini, D. Busquets Mataix and A. Tommasi, *Nanowires Implementations and Applications*, book edited by Abbass Hashim 2011, 223-244, InTech, ISBN 978-953-307-318-7 DOI: 10.5772/17155.

9 F. Abreu Araujo, M. Darques, K. A. Zvezdin, A. V. Khvalkovskiy, N. Locatelli, K. Bouzehouane, V. Cros and L. Piraux, Microwave Signal Emission in Spin-torque Vortex Oscillators in Metallic Nanowires: Experimental Measurements and Micromagnetic Numerical Study, *Phys. Rev. B,* 2012, **86**, 064424.

10 A. Hultgren, M. Tanase, E. J. Felton, K. Bhadriraju, A. K. Salem, C.S. Chen and D. H. Reich, Optimization of Yield in Magnetic Cell Separations Using Nickel Nanowires of Different Lengths, *Biotechnol. Prog*, 2005, **21**, 509-515.

11 Y. Sun, L. Hao, C. L. Chien and P. C. Searson, Tuning the Properties of Magnetic Nanowires, *IBM J. Res. Dev.* 2005, **49**, 79–102.

12 H. Zheng, J. Wang, S. E. Lofland, Z. Ma, L. Mohaddes-Ardabili, T. Zhao, L. Salamanca-Riba, S. R. Shinde, S. B. Ogale, F. Bai, D. Viehland, Y. Jia, D. G. Schlom, M. Wuttig, A. Roytburd and R. Ramesh, Multiferroic $BaTiO_3$-$CoFe_2O_4$ Nanostructures, *Science* 2004, **303**, 661-663.

13 J. Ma, J. Hu, Z. Li and C. W. Nan, Recent Progress in Multiferroic Magnetoelectric Composites: from Bulk to Thin Films, *Adv. Mater.* 2011, **23**, 062-1087.

14 F. Yao, L. Xu, B. Lin and G. D. Fuet, Preparation and Applications of Functional Nanofibers Based on the Combination of Electrospinning, Controlled Radical Polymerization and 'Click Chemistry', *Nanoscale* 2010, **2**, 1348-1357.

15 S. Xie, F. Ma, Y. Liu and J. Li, Multiferroic $CoFe_2O_4$–$Pb(Zr_{0.52}Ti_{0.48})O_3$ Core-shell Nanofibers and their Magnetoelectric Coupling, *Nanoscale* 2011, **3**, 3152-3158.

16 X. L. Liu., M. Y. Li, Z. Q. Hu, Y. D. Zhu, S. Dong and X. Z Zhao, Preparation and Properties of the $CoFe_2O_4$/$Bi_{3.15}Nd_{0.85}Ti_3O_{12}$ Multiferroic Composite Coaxial Nanotubes, *Mater. Lett.* 2012, **82** 57-60.

17 X. L. Liu, M. Y. Li, J. Wang, Z. Q. Hu, Y. D. Zhu, and X. Z. Zhao, Preparation and Characterization of Multiferroic $CoFe_2O_4$/$Bi_{0.97}Ce_{0.03}FeO_3$ Coaxial Nanotubes, *Appl. Phys. A* 2012, **108**, 829-834.

18 M. Liu, X. Li, H. Imrane, Y. Chen, T. Goodrich, Z. Cai, K. S. Ziemer, J. Y. Huang and N. X. Sun, Synthesis of Ordered Arrays of Multiferroic $NiFe_2O_4$-$Pb(Zr_{0.52}Ti_{0.48})O_3$ Core-shell Nanowires *Appl. Phys. Letters,* 2007, **90,** 152501.

19 S. H. Johnson, P. Finkel, O. D. Leaffer, S. S. Nonnenmann and K. Bussman, Magneto-elastic Tuning of Ferroelectricity within a Magnetoelectric Nanowire, *Appl. Phys. Letters* 2011, **99**, 182901.

20 T. Narayanan, B. Mandal, A. K. Tyagi, A. Kumarasiri, X. Zhan, M. G. Hahm, M. R. Anantharaman, G. Lawes and P. M. Ajayan, Hybrid Multiferroic Nanostructure with Magnetic–Dielectric Coupling, *Nano Letters*, 2012, **12**, 3025-3030.

21 A. Hernandez, K. Chang and E. Fisher, Sol–Gel Template Synthesis and Characterization of $BaTiO_3$ and $PbTiO_3$ Nanotubes, *Chem. Mater* 2002, **14**, 480-482.

22 Z. L. Xiao, C. Y. Han, U. Welp, H. H. Wang, W. K. Kwok, G. A. Willing, J. M. Hiller, R. E. Cook, D. J. Miller and G. W. Crabtree, Fabrication of Alumina Nanotubes and Nanowires by Etching Porous Alumina Membranes, *Nano Letters,* 2002, **2** *(11)*, 1293-1297.

23 J. De La Torre Medina, M. Darques and L. Piraux, Strong Low Temperature Magnetoelastic Effects in Template Grown Ni Nanowires, *J. Phys. D: Appl. Phys*. 2008, **41**, 032008.

24 H. Pan, B. Liu, J. Yi, C. Poh, S. Lim, J. Ding, Y. Feng, C. H. A. Huan and J. Lin, Growth of Single-Crystalline Ni and Co Nanowires via Electrochemical Deposition and Their Magnetic Properties, *J. Phys. Chem. B* **2005***, 109*, 3094-3098.

25 A. Encinas-Oropesa, M. Demand, L. Piraux, E. Huynen and U. Ebels, Dipolar Interactions in Arrays of Nickel Nanowires Studied by Ferromagnetic Resonance, *Phys. Rev.* B, 2001, **63**, 104415.

26 F. Zighem, T. Maurer, F. Ott and G. Chaboussant, Dipolar Interactions in Arrays of Ferromagnetic Nanowires: a Micromagnetic Study, *J. Appl. Phys*. **2011**, *109*, 013910.

27 M. Darques, A. Encinas, L. Vila and L. Piraux, Tailoring of the c-axis Orientation and Magnetic Anisotropy in Electrodeposited Co Nanowires, *J. Phys.: Cond. Matt.* 2004, **16**, S2279.

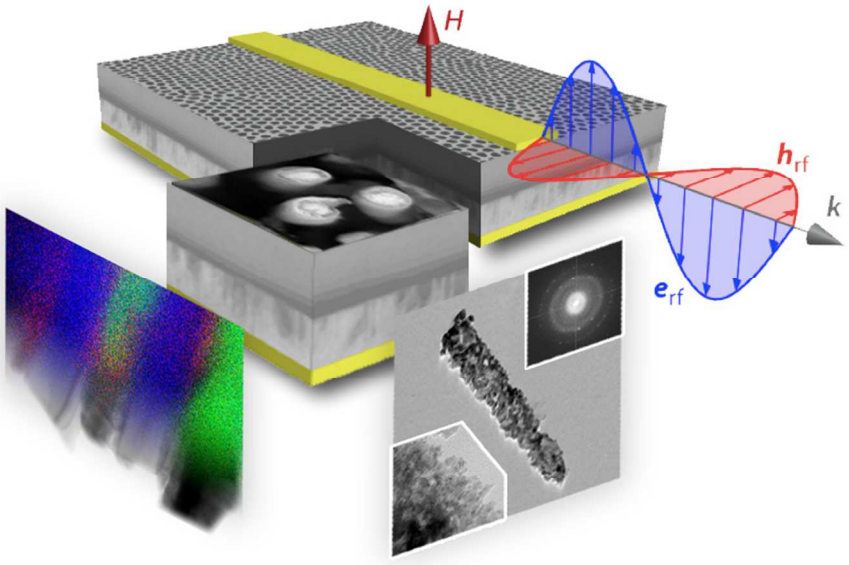

347x347mm (72 x 72 DPI)

Modulation of magnetic properties and magnetoelectric coupling enhancement provided by ferromagnetic (Ni) / dielectric ($BaTiO_3$) coaxial nanocable arrays